European Journal of Radiology 120 (2019) 108672

Contents lists available at ScienceDirect

European Journal of Radiology

journal homepage: www.elsevier.com/locate/ejrad

Research article

Intravoxel incoherent motion MR imaging for differentiating malignant lesions in spine: A pilot study

Yanjun Chen[a,b,1], Qinqin Yu[b,1], Luciana La Tegola[c], Yingjie Mei[d], Jialing Chen[a], Wenhua Huang[b], Xiaodong Zhang[a,*], Giuseppe Guglielmi[c]

[a] Department of Medical Imaging, The Third Affiliated Hospital of Southern Medical University (Academy of Orthopedics. Guangdong Province), Guangzhou, China
[b] Institute of Clinical Anatomy, School of Basic Medical Sciences, Southern Medical University, Guangzhou, China
[c] Università degli Studi di Foggia, Scuola di Specializzazione di Area Medica, Department of Radiology, Foggia, Italy
[d] Philips Healthcare, Guangzhou, China

ARTICLE INFO

Keywords:
Diffusion magnetic resonance imaging
Intravoxel incoherent motion (IVIM) MRI
Diffusion-weighted imaging (DWI)
Chemical shift imaging (CSI)
Compression fracture
Tuberculous spondylitis

ABSTRACT

Purpose: To determine the diagnostic potential of Intravoxel Incoherent Motion (IVIM) MRI for differentiating malignant spinal tumours from acute vertebral compression fractures and tuberculous spondylitis, and to compare IVIM with diffusion-weighted imaging (DWI) and chemical shift imaging (CSI).

Methods: The Institutional Review Board approved this prospective study, and informed consent was obtained. IVIM MRI, DWI, and CSI at 1.5 T were performed in 25 patients with 12 acute compression fractures, 14 tuberculous spondylitis, and 18 malignant spinal tumours. The parameters of these techniques were assessed using the Kruskal–Wallis test. The diagnostic performance of the parameters was evaluated using receiver operating characteristic (ROC) analysis.

Results: ADC, SIR, D_{slow}, D_{fast}, and *f* values of malignant tumours were significantly different from those of acute compression fracture (for all, $p < 0.05$). The mean D_{slow} and D_{fast} values of malignant spinal tumours had significant differences compared with those of tuberculous spondylitis (for all, $p < 0.05$). However, no significant differences were observed in any quantitative parameters between the acute compression fracture and the tuberculous spondylitis ($p > 0.05$). D_{slow}•*f* showed the highest AUC value of 0.980 (95%CI: 0.942–1.000) in differentiating acute compression fracture and malignant spinal tumours. D_{slow} showed the highest AUC value of 0.877 (95%CI: 0.713-0.966) in differentiating tuberculous spondylitis and malignant spinal tumours.

Conclusions: IVIM MR imaging may be helpful for differentiating malignant spinal tumours from acute vertebral compression fractures and tuberculous spondylitis.

1. Introduction

Common disorders in clinical settings are represented by spinal diseases typically caused by trauma, osteoporosis, infection, or tumours, among other factors; their diagnoses mainly depend on imaging findings and clinical features. However, benign and malignant spinal lesions may appear similar on imaging features, particularly in the early stages of the disease, making complicated the clinical treatment [1]. In the early stage or atypical spinal tuberculosis, when there is no typical significant bone erosion or abscess, the imaging findings are more complicated and sometimes are similar to those of tumors or common fractures leading to misdiagnosis. Although this is not common, it is still necessary to find ways to avoid it. Furthermore, spinal neoplasms or infections can be accompanied with compression fractures, and due to the presence of hemorrhage, the MR signal changes of acute vertebral fractures are also complicated and have some overlap of image features between different diseases. Effective differential diagnosis methods to identify different lesions in the spine have important implications for clinical practice.

It has been reported that diffusion-weighted imaging (DWI) and chemical shift imaging (CSI) is helpful for differentiating benign from malignant spinal lesions [2–6]. However, their parameters apparent

Abbreviations: IVIM, intravoxel incoherent motion; DWI, diffusion-weighted imaging; CSI, chemical shift imaging; ADC, apparent diffusion coefficient; SIR, signal intensity ratio; D_{slow}, molecular diffusion coefficient; D_{fast}, perfusion-related diffusion; f, perfusion fraction; ROC, receiver operating characteristic; AUC, area under curve

* Corresponding author.
E-mail address: ddautumn@126.com (X. Zhang).

[1] Yanjun Chen and Qinqin Yu contributed equally to this work.

https://doi.org/10.1016/j.ejrad.2019.108672
Received 1 February 2019; Received in revised form 22 August 2019; Accepted 14 September 2019

diffusion coefficient (ADC) and signal intensity ratio (SIR) have limitations for differentiating infections and malignancies [7,8]. The role of these methods in differentiating malignant tumours, infections, and compression fractures still need further study.

The intravoxel incoherent motion (IVIM) MRI has recently been demonstrated to be an attractive approach for the assessment of tissue water diffusivity and micro-capillary perfusion using signal decay at large (200–1000 s/mm^2) and relatively small (0–200 s/mm^2) b values, respectively [9,10]. Both water molecular diffusion and perfusion-related diffusion can be monitored by allowing the extraction of the molecular diffusion coefficient (D_{slow}), the perfusion-related diffusion (D_{fast}), and the perfusion fraction (*f*). The IVIM-derived quantitative parameters have been widely used in studies of the central nervous system and abdomen to more precisely assess the early diagnosis and differentiation of diseases and in the follow-up studies [11–17]. However, these parameters are less frequently used to assess musculoskeletal diseases [18–20]. Bourillon et al. [18] reported that IVIM parameters are helpful for assessing the treatment effect of multiple myeloma lesions. Marchand et al. [19] studied the feasibility of IVIM for assessing bone marrow. Zhao et al. [20] reported that IVIM-DWI plays an important role in detecting disease activity in ankylosing spondylitis patients.

Accordingly, the purpose of this study was to characterize the ADC, SIR and IVIM parameters in spinal diseases and to determine the diagnostic efficacies of IVIM for differentiating malignant spinal tumours from acute vertebral compression fractures and tuberculous spondylitis.

2. Materials and methods

2.1. Patients

The protocol of this prospective study was approved by the Ethics Committee of our hospital, and informed consent was obtained from all patients prior to the examination.

From January 2017 to October 2017, 25 consecutive patients were enrolled in this study and underwent MRI examinations of the spine, including IVIM, DWI, and CSI. The inclusion criteria for this study were as follows: 1) with clinically definitive diagnosis or histopathological diagnosis; 2) without preexisting systemic disease (such as diabetes, or metabolic disorder); 3) received no previous medication therapy that could affect bone metabolism; and 4) had no implants contraindicated for MRI examinations. The exclusion criteria were as follows: 1) retained metal in anywhere of the body; 2) had claustrophobia; 3) could not keep still during examinations; and 4) not clinically diagnosed.

10 patients with acute compression fractures were confirmed by a history of trauma and MRI examinations (six cases within 24 h and four cases within one week of injury) with high-signal intensity using fat-suppressed T_2-weighted images (T_2WI). All these 10 patients were followed-up for at least 3 months in the clinic to confirm the diagnosis. 7 patients with tuberculosis spondylitis were confirmed by histopathology with evidence of acid-fast bacilli, and they received no treatments before the MRI examinations. 8 patients with malignant spinal tumours, including five cases of metastatic tumours (primary tumours included two cases of lung cancer, two cases of prostatic carcinoma and one case of a large cell neuroendocrine carcinoma); two cases of lymphoma; and one case of multiple myeloma, were confirmed by pathological examination. A total of 44 spinal skeletal lesions in 25 patients were divided into three groups: acute compression fracture group (n = 12), tuberculous spondylitis group (n = 14) and malignant spinal tumour group (n = 18).

2.2. MR image acquisition

MRI studies were performed with a 1.5 T MRI system (Philips Achieva, the Netherlands) using a 15-channel spinal coil. Conventional MR sequences were performed using the following imaging parameters: sagittal T_2WI with a repetition time (TR) of 4000 ms, echo time (TE) of 100 ms, field of view (FOV) of 180 mm × 180 mm, slice thickness of 4 mm, slice gap of 1 mm, number of signal averages (NSA) of 2, and acquisition time of 72 s and sagittal T_1-weighted images with a TR of 600 ms, TE of 8 ms, FOV of 180 mm × 180 mm, section thickness of 4 mm, section gap of 1 mm, NSA of 2, and acquisition time of 90 s. IVIM-DWI was obtained with a sagittal spin-echo echo-planar-imaging sequence, and the parameters were as follows: b values of 0, 10, 20, 40, 80, 100, 200, 400, and 600 s/mm^2; FOV of 180 mm × 180 mm; matrix of 72 × 59; section thickness of 4 mm; section gap of 1 mm; NSA of 8; and acquisition time of 600 s. Conventional DWI was performed with two b values of 0 s/mm^2 and 600 s/mm^2, FOV of 180 mm × 180 mm; matrix of 72 × 59; section thickness of 4 mm; section gap of 1 mm; NSA of 3, and acquisition time of 170 s. CSI was obtained with a sagittal dual-echo fast field echo sequence. The parameters were as follows: TR of 150 ms, out-phase TE of 2.3 ms, in-phase TE of 4.6 ms, FOV of 250 mm × 230 mm, matrix of 132 × 133, section thickness of 3.2 mm, section gap of 0 mm, NSA of 1, and acquisition time of 20 s.

2.3. Post-processing and data analysis

All data were transferred to an imaging workstation (Extended MR workstation, Philips) for analysis. The measurements for each parameter were independently done by two radiologists with experiences for more than 5 years. The ADC value was obtained by using all b values monoexponentially fitted to the following equation: $Sb = S_0 \exp(-b \cdot ADC)$, where S_b is the signal intensity observed in the absence of a diffusion gradient. The signal intensity (SI) of each lesion was measured on the in-phase and out-phase images, and the SIR value was calculated as follows: $SIR = SI_{out\text{-}phase}/SI_{in\text{-}phase}$. The IVIM DWI data were post-processed using PRIDE software (Phillips Medical Systems, Best, The Netherlands) and measured using Image J software (National Institutes of Health, Bethesda, MD, USA). The IVIM-derived parameters were calculated consecutively by using a nonlinear biexponential fit based on the following equation: $S_b/S_0 = (1\text{-}f)\cdot\exp(-bD_{slow}) + f\exp(-bD_{fast})$, where S_0 is the mean signal intensity, D_{slow} is the molecular diffusion coefficient, D_{fast} is the perfusion-related coefficient, and *f* is the perfusion fraction. The region of interest (ROI) was set in the centre of the lesion with an area of 30–100 mm [2] and was as large as possible avoiding necrosis, bone cortex, and blood vessels. Three ROIs were placed for each lesion in different slices, the average of the ROI measurements for each parameter was used as a representative value.

2.4. Statistical analysis

All measurements were documented and saved in Excel (Microsoft, Redmond, WA, USA). All analyses were performed using SPSS 23.0 (IBM SPSS, Armonk, NY). Numerical data are reported as the mean ± standard deviation (SD) of all measurements. The intraclass correlation coefficient (ICC) was used to assess intraobserver variability using reliability analysis. nonparametric tests were used for the comparison of differences between groups the Kruskal-Wallis test with a pairwise comparison using the Mann-Whitney U test.

Nonparametric receiver operating characteristic (ROC) analysis was performed to evaluate the diagnostic performance of the ADC, CSI, and IVIM parameters. The areas under the ROC curve (AUC) were compared for significant differences between these parameters, and cut-off value for each parameter was determined by maximizing the sum of the sensitivity and specificity (the Youden index). ROC analysis was performed using MedCalc software. All statistical analyses were performed using SPSS 19.0. A p value < 0.05 was considered statistically significant.

3. Results

There were 12 vertebral body in 10 (40%) patients with acute

Table 1
Patient Demographics.

Patient group	No. of patients	No. of vertebral	Mean age (yrs)[a]	BMI
Fracture	10	12	59.70 ± 12.77	23.1 ± 2.7
Male	7	8	55.29 ± 11.91	23.3 ± 3.2
Female	3	4	70.00 ± 9.00	22.0 ± 2.5
Tuberculous Spondylitis	7	14	55.00 ± 17.02	22.8 ± 2.7
Male	4	8	64.25 ± 9.22	23.1 ± 1.2
Female	3	6	42.67 ± 18.50	22.4 ± 4.3
Malignant	8	18	57.63 ± 17.94	22.7 ± 2.9
Male	3	5	67.00 ± 14.73	22.7 ± 3.4
Female	5	13	52.00 ± 18.69	22.7 ± 3.3

Note: [a]Data are means ± standard deviations ; BMI: Body Mass Index.

compression fracture (mean age, 60 years, age range, 41–79 years), 14 vertebral body in 7 (28%) patients with tuberculous spondylitis (mean age, 55 years, age range, 31–78 years), and 18 vertebral body in 8 (32%) patients with malignant spinal tumour (mean age, 58 years, age range, 30–80 years). The descriptive statistics regarding the demographic data obtained in patients are summarized in Table 1. Figs. 1–3 shows IVIM, DWI and CSI imaging and the measurement methods for representative cases of fractures, tuberculosis, and malignant tumors.

3.1. Intraobserver reproducibility for MRI measurement

Excellent intraobserver (observer 1 and observer 2) reproducibility was obtained for ADC, SIR, D_{slow}, D_{fast}, and *f* values, with ICC value was 0.874 (95%CI: 0.79 to 0.95), 0.885 (95%CI: 0.76–1.05), 0.924 (95%CI: 0.89 to 0.97), 0.932 (95%CI: 0.92 to 0.98) and 0.902 (95%CI: 0. 85 to 0.96), respectively.

3.2. Comparison of the ADC, SIR, and IVIM parameters among the three groups

Mean values of ADC, SIR, D_{slow}, D_{fast}, and *f* values of acute vertebral compression fractures, tuberculous spondylitis, and malignant spinal tumours are described in Table 2. The results showed the mean ADC, SIR, D_{slow}, D_{fast}, and *f* values of malignant tumours were significantly different from that of acute compression fracture ($p < 0.001$). The mean D_{slow} and D_{fast} values of malignant tumours had significant differences compared with tuberculous spondylitis. However, no significant differences were found between the ADC, SIR and *f* values of tuberculous spondylitis and malignant tumours ($p > 0.05$). There were no significant differences in any quantitative parameters between the acute compression fracture and the tuberculous spondylitis ($p > 0.05$).

3.3. Comparison of diagnostic performance for differentiating acute compression fractures and malignant spinal tumours

Table 3 summarizes the ROC curve analysis results of all parameters for differentiating acute compression fracture and malignant spinal tumours. The results shows D_{slow}•*f* had the highest AUC value of 0.980 (95%CI: 0.942–1.000), followed by D_{slow} (0.866, 95%CI: 0.688-0.963), *f* (0.854, 95%CI: 0.673-0.956), ADC (0.848, 95%CI: 0.667-0.954), SIR (0.783, 95%CI: 0.591-0.913), and D_{fast} (0.727, 95%CI: 0.531-0.875). In the pairwise comparison of ROC curves between the parameters for differentiating acute compression fractures and malignant spinal tumours, D_{slo}•*f* showed much higher AUC than D_{slow}, *f*, ADC, SIR, and D_{fast} (for all, $p < 0.001$). By using the D_{slo}•*f* as a discriminative index for the discrimination of malignant spinal tumours from acute compression fractures, the sensitivity, specificity, positive likelihood ratio and negative likelihood ratio were 90.9% (95%CI: 58.7%–99.8%), 94.4% (95%CI: 72.7%–99.9%), 16.36 (95%CI: 2.4–110.9), 0.096 (95%CI: 0.01-0.6), respectively.

3.4. Comparison of diagnostic performance for differentiating tuberculous spondylitis and malignant spinal tumours

Table 4 summarizes the ROC curve analysis results of all parameters for differentiating tuberculous spondylitis and malignant spinal tumours. The results show D_{slow} had the highest AUC value of 0.877 (95%CI: 0.713-0.966), followed by D_{slow}•ADC (0.825, 95%CI: 0.676-

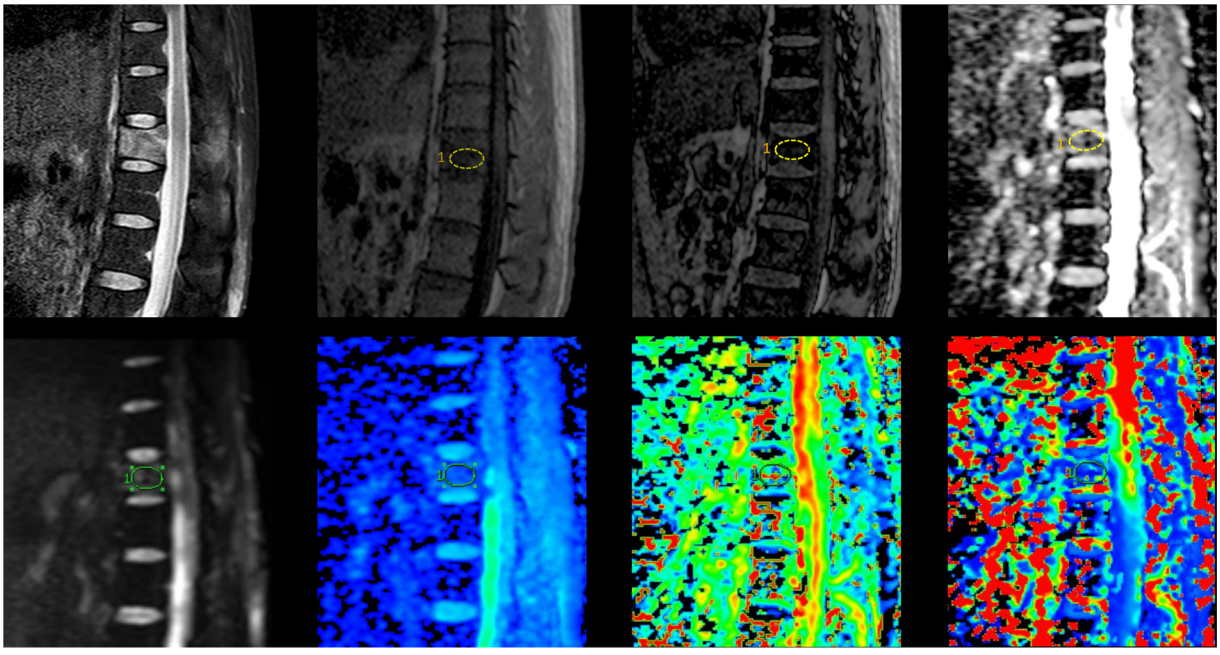

Fig. 1. A 46-year-old man with an acute compression fracture caused by trauma. The T12 lesion showed hyperintensity on T_2WI with fat suppression (a, arrow), hypointensity on the in-phase image (b) and the out-phase image (c) with a SIR value of 0.73. The lesions showed hyperintensity on the ADC map (d), and the ADC value was1.56×10^{-3} mm^2/s. ROI was placed on T_2WI (e) and then copied it to the other IVIM parametric maps of D_{slow}, *f* and D_{fast} (f–h), with values of 1.07×10^{-3} mm^2/s, 0.22, and 51.5×10^{-3} mm^2/s, respectively.

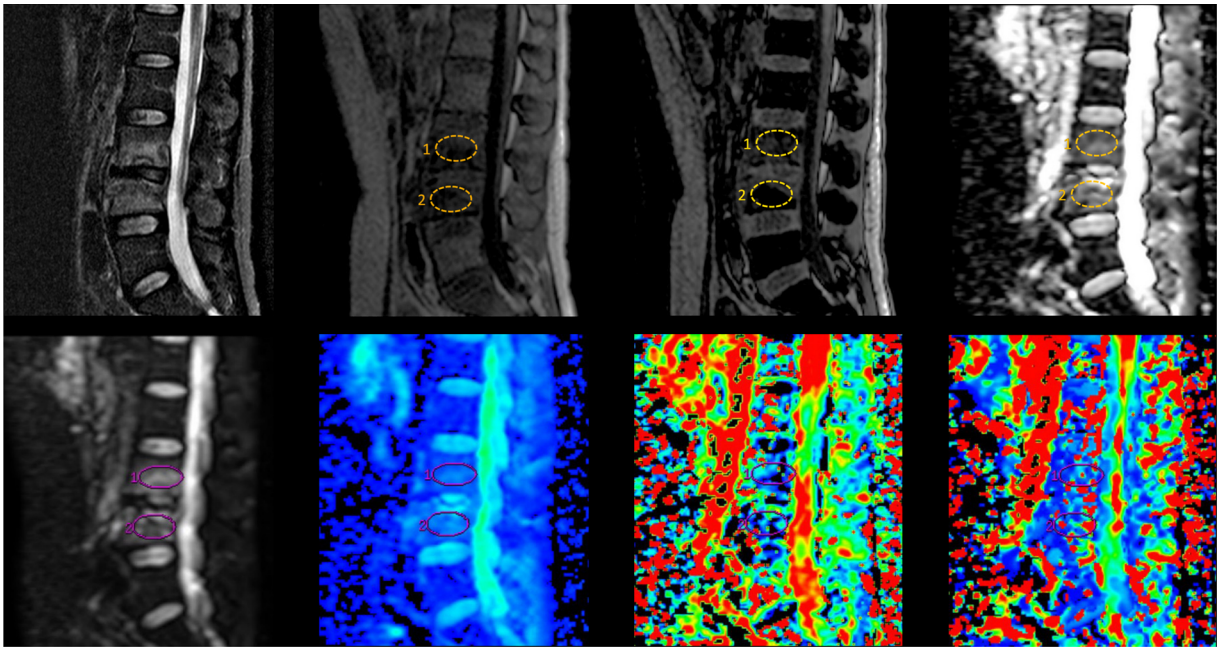

Fig. 2. A 31-year-old woman with tuberculous spondylitis of the L3-L4. The lesions showed hyperintensity on T_2WI (a, arrow). On the in-phase image (b), the lesions showed hypointensity, but they showed slight hyperintensity on the out-phase image (c) with SIR values of 1.11 (L3 lesion) and 0.99 (L4 lesion). The lesions showed hyperintensity on the ADC map (d), and the ADC values were 1.37×10^{-3} mm^2/s (L3 lesion) and 1.3×10^{-3} mm^2/s (L4 lesion). ROI was placed on T_2WI (e) and copied it to the other IVIM parametric maps of D_{slow}, f and D_{fast} (f–h) with values of 1.2×10^{-3} mm^2/s, 0.07, and 93.17×10^{-3} mm^2/s (L3 lesion) and 1.06×10^{-3} mm^2/s, 0.07, and 81.53×10^{-3} mm^2/s (L4 lesion), respectively.

0.975), ADC (0.760, 95% CI: 0.577-0.892), D_{fast} (0.758, 95%CI: 0.575-0.891), f (0.663, 95%CI: 0.475-0.819), and SIR (0.625, 95%CI: 0.437-0.789). In the pairwise comparison of ROC curves between the parameters, D_{slow} showed higher AUC than D_{slow}•ADC, ADC, D_{fast}, f, and SIR (for all, $p < 0.001$). By using the D_{slow} as a discriminative index for the discrimination of malignant spinal tumours from acute compression fractures, the sensitivity, specificity, positive likelihood ratio and negative likelihood ratio were 77.8% (95%CI: 52.4%–93.6%), 92.9% (95%CI: 66.1%–99.8%), 10.89 (95%CI: 1.6–73.2), 0.24 (95%CI: 0.1-0.6), respectively.

4. Discussion

IVIM-DWI based on the bi-exponential model was performed using

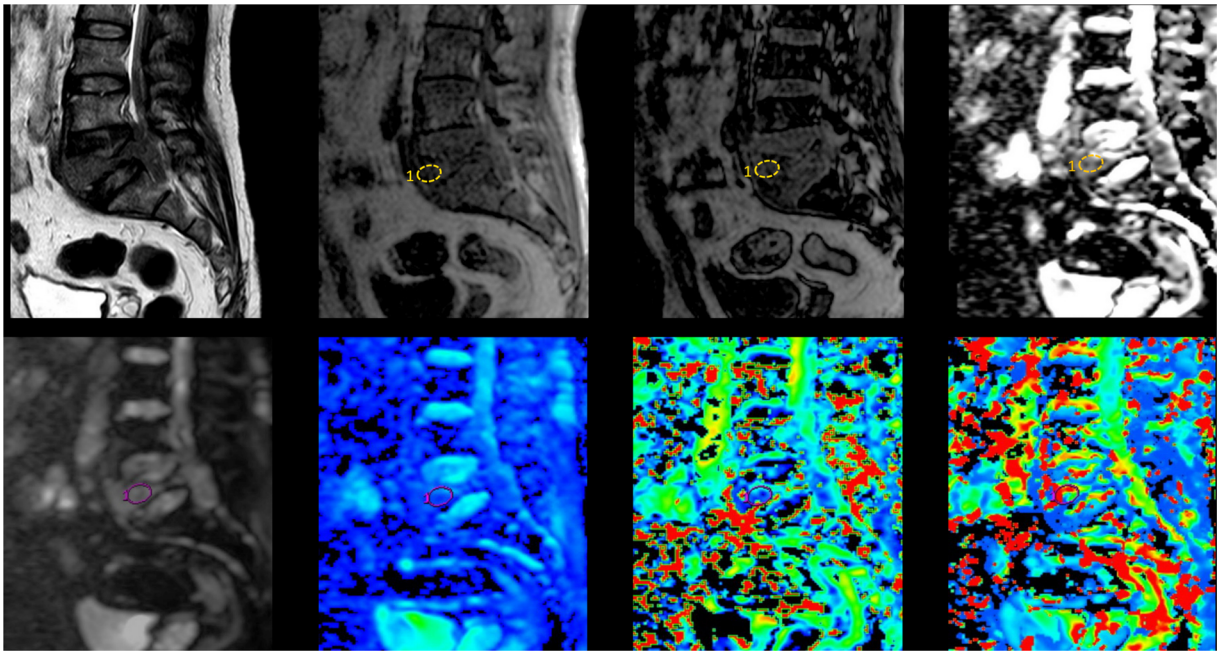

Fig. 3. A 51-year-old man with bone metastasis of the L5. The lesions showed moderate intensity on T_2WI (a, arrow). On the in-phase image (b), the lesions showed hypointensity, but they showed slight hyperintensity on the out-phase image (c) with a SIR value of 0.89. The lesions showed moderate hyperintensity on the ADC map (d), and the ADC value was 0.76×10^{-3} mm^2/s. ROI was set on T_2WI (e) and copied into the other IVIM parametric maps of D_{slow}, f and D_{fast} (f–h) with values of 0.67×10^{-3} mm^2/s, 0.08, and 136.81×10^{-3} mm^2/s, respectively.

Table 2
IVIM, DWI, and SIR parameters among the three grups.

Group	D_{slow} ($\times 10^{-3}$ mm^2/s)	*f*	D_{fast} ($\times 10^{-3}$ mm^2/s)	ADC ($\times 10^{-3}$ mm^2/s)	SIR
Acute benign compression fractures	1.25 ± 0.45	0.16 ± 0.06	102.43 ± 30.46	1.38 ± 0.52	0.87 ± 0.28
Tuberculous spondylitis	1.16 ± 0.21	0.11 ± 0.06	102.79 ± 18.78	1.22 ± 0.31	1.06 ± 0.11
Malignant tumour	0.78 ± 0.25	0.08 ± 0.03	124.11 ± 25.07	0.99 ± 0.31	1.13 ± 0.17

Table 3
ROC curves for differentiating acute benign compression fractures and malignant spinal tumours.

Parameters	IVIM				ADC ($\times 10^{-3}$ mm^2/s)	SIR
	D_{slow} ($\times 10^{-3}$ mm^2/s)	*f*	D_{fast} ($\times 10^{-3}$ mm^2/s)	D_{slow}•*f*		
AUC (95%CI)	0.866 (0.688-0.963)	0.854 (0.673-0.956)	0.727 (0.531-0.875)	0.980 (0.845-1.000)	0.848 (0.667-0.954)	0.783 (0.591-0.913)
Cutoff	0.74	0.12	98.44	0.11	0.98	0.95
SE	66.7	94.4	94.4	90.9	77.8	83.3
(95%CI)	(41.0-86.7)	(72.7-99.9)	(72.7 - 99.9)	(58.7 - 99.8)	(52.4-93.6)	(58.6-96.4)
SP	100.0	72.7	63.6	94.4	100.0	72.7
(95%CI)	(71.5-100.0)	(39.0-94.0)	(30.8 - 89.1)	(72.7 - 99.9)	(71.5-100.0)	(39.0-94.0)
+LR (95%CI)	0.00	3.46 (1.3-9.1)	2.60 (1.2 - 5.7)	16.36 (2.4 - 110.9)	0.00	3.06 (1.1-8.2)
-LR (95%CI)	0.33 (0.2-0.6)	0.076 (0.01-0.5)	0.087 (0.01 - 0.6)	0.096 (0.01 - 0.6)	0.22 (0.09-0.5)	0.23 (0.08-0.7)

Note: SE, sensitivity; SP, specificity; +LR, positive likelihood ratio. -LR, negative likelihood ratio.

multiple b values and can be used to evaluate the true diffusion and microcirculation perfusion separately but simultaneously. It has recently reported that the IVIM parameters could aid in more precisely assessing the early diagnosis and differentiation of diseases and quantitatively monitoring the treatment effect on tumours and other disorders [21–26]. In this study, the D_{slow} value of malignant tumours was significantly lower than that of benign lesions, including acute compression fracture and tuberculous spondylitis. However, the D_{fast} value was significantly higher in malignant spinal tumours, which suggests that true diffusion of malignant tumours is restricted and perfusion greatly increases, since D_{fast} is perfusion-related coefficient and is capable of providing perfusion information. For the differentiation of acute compression fractures and malignant spinal tumours, D_{slow}•*f* had the highest AUC of 0.980 (95%CI: 0.942–1.000). Using an optimum cutoff value of D_{slow}•*f* equal to 0.109 × 10^{-3} mm^2/s, we obtained the highest sensitivity of 90.9%, specificity of 94.4%. For the differentiation of tuberculous spondylitis and malignant spinal tumours, D_{slow} had the highest AUC value of 0.877 (95%CI: 0.713-0.966). With an optimum cut-off value of D_{slow} equal to 0.99 × 10^{-3} mm^2/s, the sensitivity, specificity was 77.8%, 92.9%, respectively.

Conventional DWI is based on the micro-movement of water molecules, which reflects the speed of water diffusion in the tissue. DWI is performed using two b values, one of which is 0, and imaging depends on the ADC of the organization. ADC values can be used to quantitatively assess the diffusion of the tissue, which shows microscopic changes at the cellular level caused by pathophysiological changes. However, the signal attenuation on the DWI images includes true water diffusion and microcirculation perfusion in the capillary vessels, and the latter results in a false diffusion signal on the DW images. Thus, the use of the ADC value is restricted [27,28]. The usefulness of ADC values for differentiating benign and malignant spinal diseases depends on the imaging sequence and b values and not on the subjects [29,30]. Our results showed that no significant differences were found ($p > 0.05$) between the ADC values of tuberculous spondylitis and malignant tumours as well as tuberculous spondylitis and acute compression fracture, indicating that there was ADC overlap in distinguishing tuberculous spondylitis, malignant tumours, and compression fracture. Therefore, the results suggest that conventional DWI with the ADC has limited usefulness for differentiating benign and malignant spinal lesions, which is consistent with the previous studies [7,28]. D_{slow} and *f* values except for D_{fast} value showed better diagnostic performance than ADC value for differentiating acute compression

Table 4
ROC curves for differentiating tuberculous spondylitis and malignant spinal tumours.

Parameters	IVIM				ADC ($\times 10^{-3}$ mm^2/s)	SIR
	D_{slow} ($\times 10^{-3}$ mm^2/s)	*f*	D_{fast} ($\times 10^{-3}$ mm^2/s)	D_{slow}•ADC		
AUC (95%CI)	0.877 (0.713-0.966)	0.663 (0.475-0.819)	0.758 (0.575-0.891)	0.825 (0.651-0.936)	0.760 (0.577-0.892)	0.625 (0.437-0.789)
Cutoff	0.99	0.13	110.06	0.66	0.97	1.09
SE	77.8	100.0	66.7	66.7	72.2	61.1
(95%CI)	(52.4-93.6)	(81.5 - 100.0)	(41.0-86.7)	(41.0 - 86.7)	(46.5-90.3)	(35.7 - 82.7)
SP	92.9	35.7	78.6	92.9	85.7	71.4
(95%CI)	(66.1-99.8)	(12.8 - 64.9)	(49.2-95.3)	(66.1 - 99.8)	(57.2-98.2)	(41.9 - 91.6)
+LR (95%CI)	10.89 (1.6-73.2)	1.56 (1.1 - 2.3)	3.11 (1.1-8.9)	9.33 (1.4 - 63.5)	5.06 (1.4-18.8)	2.14 (0.9 - 5.3)
-LR (95%CI)	0.24 (0.1-0.6)	0.00	0.42 (0.2-0.9)	0.36 (0.2 - 0.7)	0.32 (0.1-0.7)	0.54 (0.3 - 1.1)

Note: SE, sensitivity; SP, specificity; +LR, positive likelihood ratio. -LR, negative likelihood ratio.

fractures and malignant spinal tumours. When D_{slow} and *f* used in combination, their AUCs improved significantly to 0.980 (95%CI: 0.942–1.000). For the differentiation of tuberculous spondylitis and malignant spinal tumours, D_{slow} value representing the true diffusion of water outperformed other parameters, with AUC of 0.877 (95%CI: 0.713-0.966). The mean ADC value was not significantly different but had a higher AUC than D_{fast} and *f* values (AUC: 0.760 vs 0.758 vs 0.663). The reasons for the above results may be the pathophysiological changes of the diseases and the theory behind different imaging techniques. Under the influence of antibacterial treatment or immune system response, spinal TB could appear atypical imaging findings in clinical, such as affecting only a single vertebral body combined bone destruction and granulation tissue and without paraspinal abscesses or involvement of the end plates and disk spaces, can mimic neoplastic diseases. Its diagnosis was challenging and could be misdiagnosed as malignant lesions occasionally. For the differentiation of benign acute compression fractures and tuberculous spondylitis, we found that not only did the IVIM parameters and ADC show no usefulness in differentiating benign compression fractures and tuberculous spondylitis, which was in accordance with the report by Pui MH [7].

In addition, our study suggests that the AUC of the SIR value for differentiating malignant spinal tumours and tuberculous spondylitis was the lowest (0.625, 95%CI: 0.437-0.789). There was no significant difference in mean SIR between malignant spinal tumours and tuberculous spondylitis ($p > 0.05$). For the differentiation of acute compression fractures and malignant spinal tumours, SIR showed AUC of 0.783, with a wide range of 95%CI from 0.591 to 0.913. The role of the SIR in differentiating benign and malignant spinal lesions was mainly attributed to its value in differentiating benign acute compression fractures and malignant tumours rather than in differentiating tuberculous spondylitis and malignant tumours. Therefore, our study suggests that CSI with SIR value may not be very suitable for differentiating benign and malignant spinal lesions. Geith et al. [8] also reported that CSI with SIR values was not feasible for differentiating benign and malignant spinal lesions, but Douis et al. [5] suggested that CSI was useful for identifying spinal malignant skeletal lesions with high sensitivity. This discrepancy is also due to the selected subjects, and we speculate that it is based on the CSI theory and previous studies [31–36]. As mentioned above, tuberculous spondylitis can mimic a malignancy, and it also erodes normal marrow. The fat tissue in the vertebral marrow for tuberculous spondylitis decreases, but it correlates with the activity, duration and treatment of the infection. Therefore, the SIR value of infection is between that of simple benign lesions and malignancy, and it has a relatively large overlap with malignancies [8]. The SIR value indicates a lower effect for differentiating benign and malignant spinal lesions with infectious diseases in this study. The authors have recently suggested that field MRI scanners and sequences also influence signal loss in CSI, which still needs further study [37,38].

This study also has some limitations. Firstly, IVIM has been investigated only up to a b-value of 600 s/mm^2. Together with a field strength of 1.5 T this may provide relatively low sensitivity. Secondly, the overall patient number is relatively small. Thirdly, benign spinal tumours (such as haemangioma) or tumour-like lesions (such as eosinophilic granuloma) and other infectious types of spondylitis (such as fungal infection) were not included. Finally, IVIM technology itself is not stable, and the calculations still need further exploration.

In conclusion, IVIM quantitative parameters can aid in differentiating malignant tumours from acute vertebral compression fractures and tuberculous spondylitis. The combined D_{slow} and *f* parameters are better than D_{fast}, ADC and SIR, particularly for the differentiation of acute compression fractures and malignancies. The D_{slow} is better than other parameters in differentiating tuberculous spondylitis and malignant spinal tumours. IVIM may have great potential if a shorter scan time, a stabilized sequence and parameters, and optimized post-processing can be achieved. Despite the small patient population, this study may lead to further developments in the application of IVIM in differentiating benign and malignant spinal skeletal lesions.;'

Funding

This study has received funding by: 2017B090912006, The Science and Technology Planning Project of Guangdong Province; 81801653, National Natural Science Foundation of China (NSFC).

Declaration of Competing Interest

The authors have no conflict of interest to declare.

Acknowledgments

We acknowledge the help of Dr Shengli An (statistician at the Southern Medical university) with the statistical analysis. The scientific guarantor of this publication is Xiaodong Zhang.

References

[1] S.K. Thawait, M.A. Marcus, W.B. Morrison, R.A. Klufas, J. Eng, J.A. Carrino, Research synthesis: what is the diagnostic performance of magnetic resonance imaging to discriminate benign from malignant vertebral compression fractures? Systematic review and meta-analysis, Spine 37 (2012) E736–E744.
[2] J.K. Sung, W.H. Jee, J.Y. Jung, et al., Differentiation of acute osteoporotic and malignant compression fractures of the spine: use of additive qualitative and quantitative axial diffusion-weighted MR imaging to conventional MR imaging at 3.0 T, Radiology 271 (2014) 488–498.
[3] O. Dietrich, T. Geith, M.F. Reiser, et al., Diffusion imaging of the vertebral bone marrow, NMR Biomed. 30 (3) (2015).
[4] H. Rumpel, Y. Chong, D.A. Porter, L.L. Chan, Benign versus metastatic vertebral compression fractures: combined diffusion-weighted MRI and MR spectroscopy aids differentiation, Eur. Radiol. 23 (2013) 541–550.
[5] H. Douis, A.M. Davies, L. Jeys, P. Sian, Chemical shift MRI can aid in the diagnosis of indeterminate skeletal lesions of the spine, Eur. Radiol. 26 (2016) 932–940.
[6] A. Ogura, K. Hayakawa, F. Maeda, et al., Differential diagnosis of vertebral compression fracture using in-phase/opposed-phase and short TI inversion recovery imaging, Acta Radiol. 53 (2012) 450–455.
[7] M.H. Pui, A. Mitha, W.I. Rae, P. Corr, Diffusion-weighted magnetic resonance imaging of spinal infection and malignancy, J. Neuroimaging 15 (2005) 164–170.
[8] T. Geith, G. Schmidt, A. Biffar, et al., Comparison of qualitative and quantitative evaluation of diffusion-weighted MRI and chemical-shift imaging in the differentiation of benign and malignant vertebral body fractures, AJR Am. J. Roentgenol. 199 (2012) 1083–1092.
[9] D. Le Bihan, E. Breton, D. Lallemand, P. Grenier, E. Cabanis, M. Laval-Jeantet, MR imaging of intravoxel incoherent motions: application to diffusion and perfusion in neurologic disorders, Radiology 161 (1986) 401–407.
[10] D. Le Bihan, Intravoxel incoherent motion perfusion MR imaging: a wake-up call, Radiology 249 (2008) 748–752.
[11] N. Shen, L. Zhao, J. Jiang, et al., Intravoxel incoherent motion diffusion-weighted imaging analysis of diffusion and microperfusion in grading gliomas and comparison with arterial spin labeling for evaluation of tumor perfusion, J. Magn. Reson. Imaging 44 (3) (2016) 620–632.
[12] C. Federau, P. Maeder, K. O'Brien, P. Browaeys, R. Meuli, P. Hagmann, Quantitative measurement of brain perfusion with intravoxel incoherent motion MR imaging, Radiology 265 (2012) 874–881.
[13] O. Bane, M. Wagner, J.L. Zhang, et al., Assessment of renal function using intravoxel incoherent motion diffusion-weighted imaging and dynamic contrast-enhanced MRI, J. Magn. Reson. Imaging (2016), https://doi.org/10.1002/jmri.25171.
[14] X.R. Cai, J. Yu, Q.C. Zhou, et al., Use of intravoxel incoherent motion MRI to assess renal fibrosis in a rat model of unilateral ureteral obstruction, J. Magn. Reson. Imaging (2016), https://doi.org/10.1002/jmri.25172.
[15] N. Shirota, K. Saito, K. Sugimoto, K. Takara, F. Moriyasu, K. Tokuuye, Intravoxel incoherent motion MRI as a biomarker of sorafenib treatment for advanced hepatocellular carcinoma: a pilot study, Cancer Imaging 16 (1) (2016).
[16] S. Barbieri, O.F. Donati, J.M. Froehlich, H.C. Thoeny, Comparison of Intravoxel incoherent motion parameters across MR imagers and Field strengths: evaluation in upper abdominal organs, Radiology (2015) 151244.
[17] S. Ichikawa, U. Motosugi, T. Ichikawa, K. Sano, H. Morisaka, T. Araki, Intravoxel incoherent motion imaging of the kidney: alterations in diffusion and perfusion in patients with renal dysfunction, Magn. Reson. Imaging 31 (2013) 414–417.
[18] C. Bourillon, A. Rahmouni, C. Lin, et al., Intravoxel incoherent motion diffusion-weighted imaging of multiple myeloma lesions: correlation with whole-body dynamic contrast agent-enhanced MR imaging, Radiology 277 (2015) 773–783.
[19] A.J. Marchand, E. Hitti, F. Monge, et al., MRI quantification of diffusion and perfusion in bone marrow by intravoxel incoherent motion (IVIM) and non-negative least square (NNLS) analysis, Magn. Reson. Imaging 32 (2014) 1091–1096.
[20] Y.H. Zhao, S.L. Li, Z.Y. Liu, et al., Detection of active Sacroiliitis with ankylosing spondylitis through Intravoxel incoherent motion diffusion-weighted MR imaging, Eur. Radiol. 25 (2015) 2754–2763.

[21] Y. Xiao-Ping, H. Jing, L. Fei-Ping, et al., Intravoxel incoherent motion MRI for predicting early response to induction chemotherapy and chemoradiotherapy in patients with nasopharyngeal carcinoma, J. Magn. Reson. Imaging 43 (2016) 1179–1190.
[22] C. Liu, K. Wang, Q. Chan, et al., Intravoxel incoherent motion MR imaging for breast lesions: comparison and correlation with pharmacokinetic evaluation from dynamic contrast-enhanced MR imaging, Eur. Radiol. 26 (11) (2016) 3888–3898.
[23] L. Liang, W.B. Chen, K.W. Chan, et al., Using Intravoxel incoherent motion MR imaging to study the renal pathophysiological process of contrast-induced acute kidney injury in rats: comparison with conventional DWI and arterial spin labelling, Eur. Radiol. 26 (6) (2015) 1597–1605.
[24] G.Y. Cho, L. Moy, S.G. Kim, et al., Evaluation of breast cancer using Intravoxel incoherent motion (IVIM) histogram analysis: comparison with malignant status, histological subtype, and molecular prognostic factors, Eur. Radiol. 26 (8) (2015) 2547–2558.
[25] S. Nougaret, H.A. Vargas, Y. Lakhman, et al., Intravoxel incoherent motion-derived histogram metrics for assessment of response after combined chemotherapy and radiation therapy in rectal cancer: initial experience and comparison between single-section and volumetric analyses, Radiology 280 (2) (2016) 446–454.
[26] M. Iima, D. Le Bihan, Clinical Intravoxel incoherent motion and diffusion MR imaging: past, present, and future, Radiology 278 (2016) 13–32.
[27] N.E. Leeds, A.J. Kumar, X.J. Zhou, G.C. McKinnon, Magnetic resonance imaging of benign spinal lesions simulating metastasis: role of diffusion-weighted imaging, Top. Magn. Reson. Imaging 11 (2000) 224–234.
[28] J.H. Chan, W.C. Peh, E.Y. Tsui, et al., Acute vertebral body compression fractures: discrimination between benign and malignant causes using apparent diffusion coefficients, Br. J. Radiol. 75 (2002) 207–214.
[29] T. Geith, G. Schmidt, A. Biffar, et al., Quantitative evaluation of benign and malignant vertebral fractures with diffusion-weighted MRI: what is the optimum combination of b values for ADC-based lesion differentiation with the single-shot turbo spin-echo sequence? AJR Am. J. Roentgenol. 203 (2014) 582–588.
[30] A. Biffar, A. Baur-Melnyk, G.P. Schmidt, M.F. Reiser, O. Dietrich, Quantitative analysis of the diffusion-weighted steady-state free precession signal in vertebral bone marrow lesions, Invest. Radiol. 46 (2011) 601–609.
[31] R. Bitar, G. Leung, R. Perng, et al., MR pulse sequences: what every radiologist wants to know but is afraid to ask, RadioGraphics 26 (2006) 513–537.
[32] M.J. Kransdorf, M.D. Bridges, Current developments and recent advances in musculoskeletal tumor imaging, Semin. Musculoskelet. Radiol. 17 (2013) 145–155.
[33] K. Eito, S. Waka, N. Naoko, A. Makoto, H. Atsuko, Vertebral neoplastic compression fractures: assessment by dual-phase chemical shift imaging, J. Magn. Reson. Imaging 20 (2004) 1020–1024.
[34] Y. Ragab, Y. Emad, T. Gheita, et al., Differentiation of osteoporotic and neoplastic vertebral fractures by chemical shift {in-phase and out-of phase} MR imaging, Eur. J. Radiol. 72 (2009) 125–133.
[35] V. Zampa, M. Cosottini, C. Michelassi, S. Ortori, L. Bruschini, C. Bartolozzi, Value of opposed-phase gradient-echo technique in distinguishing between benign and malignant vertebral lesions, Eur. Radiol. 12 (2002) 1811–1818.
[36] D.C. Zajick Jr, W.B. Morrison, M.E. Schweitzer, J.A. Parellada, J.A. Carrino, Benign and malignant processes: normal values and differentiation with chemical shift MR imaging in vertebral marrow, Radiology 237 (2005) 590–596.
[37] F. Del Grande, T. Subhawong, A. Flammang, L.M. Fayad, Chemical shift imaging at 3 Tesla: effect of echo time on assessing bone marrow abnormalities, Skeletal Radiol. 43 (2014) 1139–1147.
[38] D. Dreizin, S. Ahlawat, F. Del Grande, L.M. Fayad, Gradient-echo in-phase and opposed-phase chemical shift imaging: role in evaluating bone marrow, Clin. Radiol. 69 (2014) 648–657.